Proceedings of the 4th International Conference on Functional Materials and Civil Engineering
DOI: 10.54254/2755-2721/2026.36569

Effects of Ambient Temperature on the Aerodynamic Performance of High-Speed Trains

Dongwei Li

School of Mechanical Engineering, University of Shanghai for Science and Technology, Shanghai, China
2837218384@qq.com

Abstract. With high-speed railway networks continuously expanding to areas with extreme cold climates, the impact of ambient temperature on the aerodynamic properties of high-speed trains has gradually become a research hotspot. This paper adopts computational fluid dynamics (CFD) numerical simulation technology to test the aerodynamic parameter variation law of high-speed trains within the temperature range of −20 °C to 20 °C. The calculation results show that air density will rise when the ambient temperature drops, which further leads to an obvious increase in the overall aerodynamic resistance of the train; the total drag value measured at −20 °C is roughly 14.9% higher than that under 20 °C working condition. Meanwhile, the downward pressure borne by the head car and the lift force of the tail car both grow, which will break the original balance state of the longitudinal pitching moment of the vehicle. The subsequent flow field analysis results indicate that low-temperature environments can expand the high-pressure stagnation area on the head car surface and strengthen the negative pressure area distributed on the train roof, and these two flow field changes are the fundamental reasons for the growth of each aerodynamic load. The research conclusions of this paper can provide reliable theoretical support for energy consumption evaluation and safe operation guarantee of high-speed trains operating in frigid zones.

Keywords: high-speed train, aerodynamic performance, temperature effect, numerical simulation, flow-field analysis

1. Introduction

The continuous improvement of the operating speed of high-speed trains makes train aerodynamics a core research factor that restricts vehicle running safety, passenger riding comfort and external environmental adaptability. In recent years, domestic and foreign scholars have carried out abundant research work on the aerodynamic characteristics of high-speed trains under various complex operating environments.

Han et al. [1] took low-temperature wind tunnel test equipment as the research carrier and explored how Reynolds number changes affect the aerodynamic performance of high-speed trains. Their test data proved that the test environment with a high Reynolds number can better restore the actual operation state of trains, which is a necessary premise to accurately predict the magnitude of

© 2026 The Authors. This is an open access article distributed under the terms of the Creative Commons Attribution License 4.0 (https://creativecommons.org/licenses/by/4.0/).

DOI: 10.54254/2755-2721/2026.36569

each aerodynamic load of vehicles. On this basis, Dai et al. [2] selected different altitude environments as research variables to carry out aerodynamic characteristic tests of high-speed trains; they analyzed the changing rule of air density and its influence on vehicle surface pressure distribution and aerodynamic force value, laying a basic research framework for follow-up aerodynamic exploration of plateau railway vehicles. Apart from environmental parameters, different operation working conditions will also change the flow field distribution around the train body. Du et al. [3] established a numerical calculation model to analyze the rainwater accumulation and flow movement state on the front windshield of high-speed trains, and clarified the interference effect of complex gas-liquid two-phase flow on the external flow field of the whole vehicle. In terms of crosswind research, Wang et al. [4] analyzed the crosswind aerodynamic load characteristics of high-speed trains running on embankment roadbeds. He et al. [5] completed wind tunnel model tests for viaduct operating conditions with turbulent crosswind inflow, and further clarified the influence of incoming flow turbulence intensity on the aerodynamic load borne by trains. Liu et al. [6] built a CFD calculation model to simulate the whole process of trains passing through windbreak transition sections under crosswind conditions, and analyzed the transient fluctuation characteristics of aerodynamic loads caused by the structural mutation of wind barrier facilities. Zhao et al. [7] supplemented the research on noise barrier facilities under crosswind environments, and verified that reasonably optimized noise barrier structures can effectively reduce the crosswind aerodynamic load of trains. Suzuki et al. [8] completed an early systematic sorting of the aerodynamic characteristics of trains under crosswind action, and put forward a set of corresponding experimental evaluation systems. Later, Suzuki and Hibino [9] combined field line measurement and wind tunnel model test data to realize mutual verification of crosswind aerodynamic characteristics, which greatly improved the engineering application value of wind tunnel test results. In addition, Zhang et al. [10] adopted detached eddy simulation (DES) numerical calculation method to capture the unsteady flow field evolution characteristics of high-speed trains under crosswind, and this method provides an effective numerical calculation means for simulating complex vortex flow structures around vehicles.

To sum up, existing domestic and international research has fully revealed the changing rules of train aerodynamic characteristics under the influence of Reynolds number, altitude, rainfall, crosswind, wind barrier and noise barrier structures. However, the internal aerodynamic mechanism of high-speed trains under different ambient temperature conditions has not been studied in depth. In particular, the evolution law of the surrounding flow field and the transmission characteristics of surface pressure under variable temperature environments still need further targeted exploration.

2. Numerical model and methodology

2.1. Geometric model and computational domain

The train geometric model used in this research adopts a full streamline design scheme that meets the aerodynamic design standard of high-speed operation, and both the front nose and rear tail are designed with rounded conical transition structures to reduce the running resistance of the vehicle. The overall geometric dimensions of the model are marked in Figure 1: total vehicle length L = 54.14 m, vehicle body width W = 3.2 m, vehicle height H = 3.89 m.

The boundary condition setting of the calculation domain follows the conventional configuration scheme of steady incompressible viscous external flow numerical simulation. The inlet surface is set as velocity inlet boundary, the incoming flow velocity is fixed at 97.22 m/s, and the turbulence intensity and hydraulic diameter parameters are matched synchronously. The left, right and top

DOI: 10.54254/2755-2721/2026.36569

boundaries of the calculation domain are set as symmetric boundaries, which can simulate the infinite uniform incoming flow environment in the actual open space. The outlet surface at the rear of the domain adopts pressure outlet boundary, and the static pressure value is set as the standard atmospheric reference pressure, so that the flow field disturbance generated by the train can flow out of the calculation domain without reflection interference. The ground boundary is set as moving wall surface, and its translation speed is consistent with the incoming flow velocity at the inlet, which can accurately restore the no-slip ground condition when the train runs in a straight line at a constant speed.

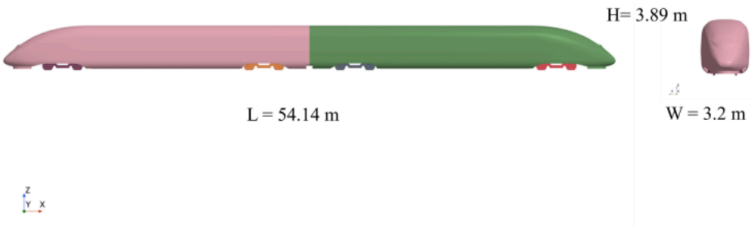

(a)

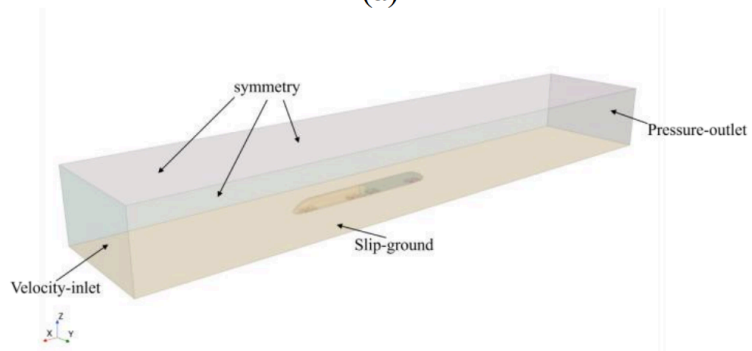

(b)

Figure 1. Train model and computational domain

2.2. Mesh generation

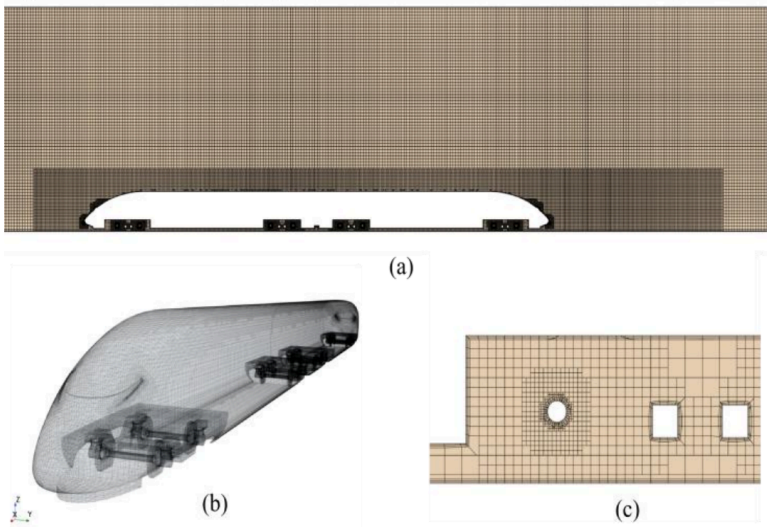

Figure 2. Mesh details

DOI: 10.54254/2755-2721/2026.36569

This paper adopts a mixed mesh zoning encryption strategy to balance the boundary layer flow capture accuracy and the overall calculation efficiency of the model. As shown in Figure 2, the far-field area far away from the train body is divided by hexahedral structured meshes. The mesh density is graded along the flow direction, wall normal direction and span direction of the train, and the mesh size is gradually increased as the distance from the vehicle body increases, so as to avoid redundant mesh quantity and reduce unnecessary calculation consumption. The surface of the train body is divided by quadrilateral surface meshes, which can well fit the complex curved surfaces of the nose, bogie and pantograph. For the underbody area with complex flow changes, local refined hexahedral meshes are arranged as shown in Figure 2(c) to ensure the orthogonality and continuity of the boundary layer mesh. The height of the first layer of mesh near the wall is calculated according to the y^+ matching standard of the SST k–ω turbulence model, and the mesh growth ratio in all spatial directions is controlled below 1.2.

2.3. Numerical method

The numerical simulation calculation of this paper is based on the three-dimensional steady incompressible Reynolds-averaged Navier–Stokes (RANS) control equations. The SST k–ω shear stress transport turbulence model is selected to close the turbulence equation; this model can accurately predict the near-wall turbulent viscosity value and reasonably describe the convection transport characteristics of the far-field flow field. The pressure-based implicit solver is used to discretize each control equation, and the SIMPLE algorithm is adopted to realize the coupled solution of pressure and velocity fields.

3. Analysis and discussion

3.1. Aerodynamic force analysis at different temperatures

The simulation calculation data show that ambient temperature has an obvious regulating effect on the aerodynamic load borne by the head car and tail car, and the statistical data of each load index are summarized in Table 1. Within the test temperature range of −20 °C to 20 °C, each aerodynamic force value of the head and tail car decreases continuously with the rise of ambient temperature. Specifically, the aerodynamic resistance of the head car drops from 7246 N to 6306 N, with a total reduction amplitude of about 13.0%; the drag of the tail car decreases from 8213 N to 7167 N. The absolute value of downward pressure on the head car decreases from 7247 N to 6297 N, with a reduction rate of approximately 15.1%; the lift force of the tail car falls from 3728 N to 3248 N. The above changing rules are determined by the coupling relationship among temperature, atmospheric pressure and air density. Under the condition of constant atmospheric pressure, the reduction of ambient temperature will directly increase air density; the dense air medium will strengthen the viscous friction effect and pressure difference effect on the surface of the train body at the same time, thus simultaneously increasing the vehicle running resistance and each aerodynamic load. In low-temperature environments, the increased downward pressure on the head car can improve the wheel-rail adhesion performance and enhance the straight-line running stability of the vehicle, but it will be accompanied by the synchronous growth of upward lift on the tail car. The enhanced tail lift will make the rear of the vehicle have an obvious floating tendency; together with the increased longitudinal aerodynamic pitching moment, it will put forward higher control requirements for the longitudinal stability of the whole vehicle.

DOI: 10.54254/2755-2721/2026.36569

Table 1. Aerodynamic force of the train

temperature (°C)	Head drag (N)	Tail drag (N)	Head lift (N)	Tail lift (N)
-20	7246	8213	-7247	3728
-10	6966	7929	-6972	3620
0	6705	7700	-6817	3499
10	6483	7458	-6600	3379
20	6306	7167	-6297	3248

3.2. Flow-field analysis

3.2.1. Velocity field

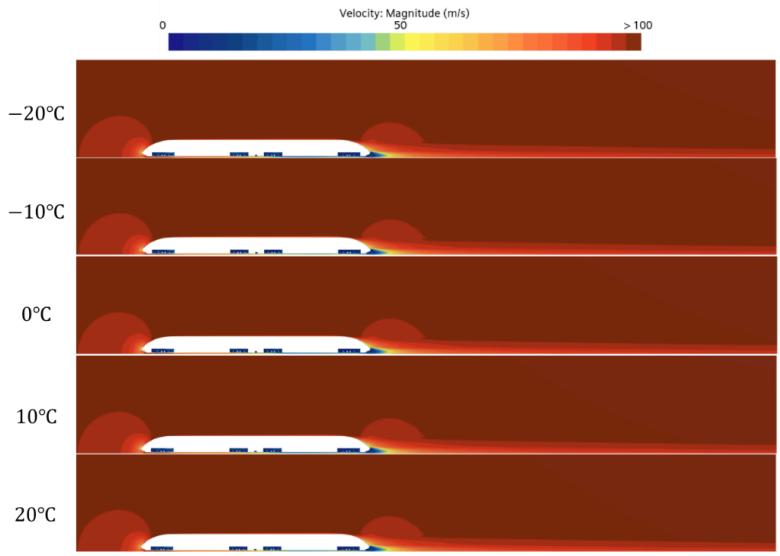

Figure 3. Velocity contours at different temperatures

It can be seen from the velocity cloud diagram in Figure 3 that a high-pressure stagnation zone will be formed at the foremost tip of the train nose under all temperature working conditions. After the air flow hits the stagnation point, it accelerates rapidly along the upper and lower surfaces of the nose, forming high-speed flow strips after flow separation around the blunt body. A large number of low-speed vortex areas appear at the bogie position under the vehicle body; the complex mechanical structure of the bogie hinders the uniform flow of air, triggers frequent flow separation and reattachment behaviors, and forms complex local flow structures with significantly lower velocity than the mainstream air flow. In the initial section of the vehicle wake, flow separation forms a low-speed mixing zone; with the backward diffusion of the wake, the internal velocity distribution presents an obvious layered structure, which reflects the mixing process of air flow at different vertical heights. Comparing the cloud diagrams under each temperature condition, the acceleration effect of the air flow around the nose is always obvious, and the overall flow velocity under the vehicle body remains at a high level. Although temperature changes will adjust the air viscosity coefficient, the influence on the macroscopic flow line topology is limited, which is mainly reflected

DOI: 10.54254/2755-2721/2026.36569

in the difference of flow velocity magnitude, and the overall structural form of the flow field does not change significantly.

3.2.2. Vorticity field and turbulent kinetic energy

Figure 4 lists the vorticity magnitude cloud diagrams of the train under five temperature working conditions. The high-vorticity areas marked by red and yellow colors are mainly distributed above each wheel set and the side skirt of the bogie. When the air flow passes through these complex mechanical structures, intense flow separation and reattachment phenomena occur, generating a large number of turbulent vortex structures. Although the overall distribution form of the high-vorticity area under each temperature is basically consistent, the coverage range and peak intensity of the high-vorticity area will increase slightly with the drop of temperature. This phenomenon may be caused by the change of air viscosity with temperature, which will shift the boundary layer separation position and adjust the turbulence intensity around the vehicle body. At the nose tip, the incoming flow accelerates and splits to both sides, forming a thin high-vorticity shear layer attached to the vehicle body surface. A fan-shaped high-vorticity diffusion area exists at the rear of the tail car, which is a typical flow feature of blunt body wake: the air flow separates at the tail end to form a large-scale low-pressure wake area, accompanied by strong vortex shedding and turbulent mixing behaviors.

The turbulent kinetic energy (TKE) cloud diagram in Figure 5 shows that the high-value turbulent kinetic energy areas are concentrated at the outlet of each bogie cavity and the internal local position of the cavity. When the air flow passes through the complex mechanical structures and gaps in the bogie cavity, it will experience repeated separation, reattachment and vortex shedding, thus generating strong turbulent fluctuation signals. The high TKE area extends backward from the cavity outlet to form an obvious turbulent wake strip, which proves that the bogie area is the main source of turbulent energy generation in the underbody flow field. Local small components in the bogie cavity will also cause a moderate rise of turbulent kinetic energy; the air flow accelerates locally through the gaps of these components and produces flow disturbance, which further increases the turbulence intensity of the surrounding flow field. In the narrow gap between the vehicle underbody and the ground, the gap extrusion effect leads to extremely high flow velocity, forming strong shear stress on the upper and lower wall surfaces of the gap, and thus forming continuous high TKE strips along the whole length of the underbody.

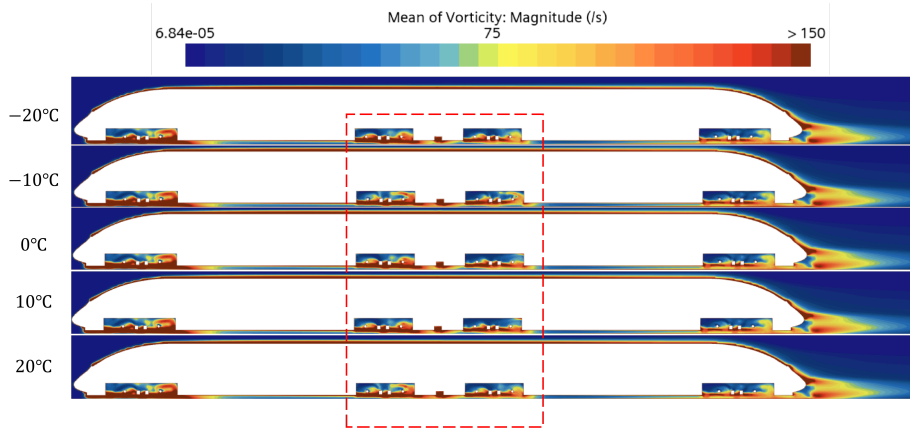

Figure 4. Vorticity magnitude contours at different temperatures

DOI: 10.54254/2755-2721/2026.36569

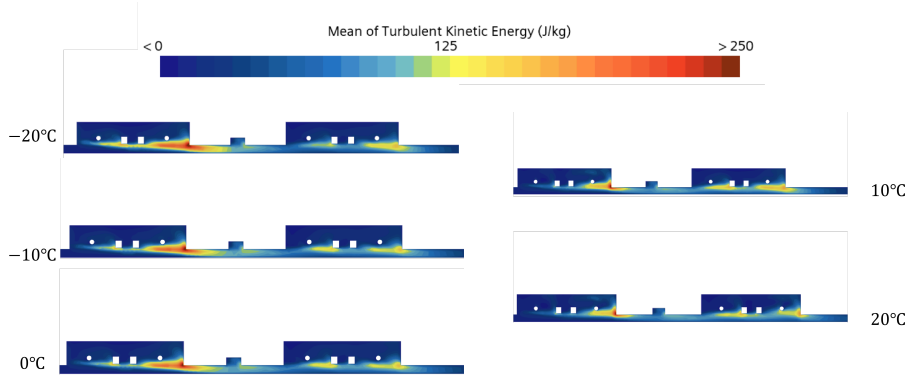

Figure 5. Comparison of turbulent kinetic energy at different temperatures

3.2.3. Pressure field

Pressure cloud diagram is an important visual basis for explaining the variation law of aerodynamic loads. As shown in Figure 6, the nose tip of the train presents a high-pressure area marked red under all temperature working conditions, while the roof and tail areas are covered with low-pressure areas. The high-pressure zone at the nose tip corresponds to the stagnation point of incoming flow impact; the kinetic energy of the air flow is converted into static pressure energy after hitting the vehicle body, forming a high-pressure concentration area. When the air flow flows backward along the conical surface of the nose, the pressure drops sharply and quickly transitions to a negative pressure area. A large range of blue negative pressure areas are distributed at the rear of the head car and both sides of the vehicle body, which is formed by the acceleration of air flow bypassing the streamlined nose. According to Bernoulli's principle, the rise of flow velocity will reduce the local static pressure, and this negative pressure distribution state directly determines the lift force and lateral stability characteristics of the train.

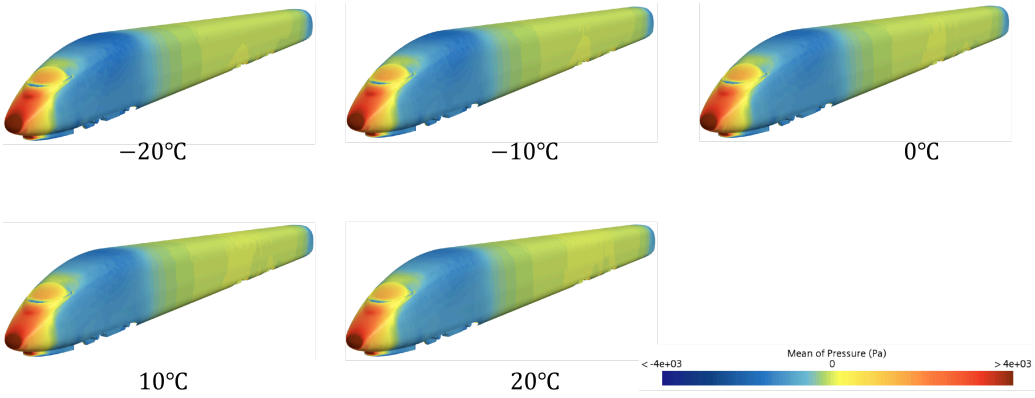

Figure 6. Comparison of surface pressure on the train at different temperatures

From the side perspective of the cloud diagram, the edge of the vehicle underbody also has local pressure fluctuation, which is mainly related to the complex bogie structure and ground flow effect. Comparing the pressure cloud diagrams under different temperature conditions, we can summarize an obvious changing rule: in low-temperature environments, the peak pressure value and coverage range of the high-pressure area on the head car surface are significantly higher than those under high-temperature conditions, and the negative pressure intensity on the roof surface is also greatly enhanced. The above flow field change characteristics provide intuitive visual evidence for the

DOI: 10.54254/2755-2721/2026.36569

conclusion in Section 3.1 that each aerodynamic load increases with the drop of ambient temperature.

4. Conclusion

This paper uses CFD numerical simulation technology to carry out aerodynamic characteristic tests of high-speed trains in the temperature interval of −20 °C to 20 °C. The main research conclusions are sorted out as follows:

1. The reduction of ambient temperature will increase air density, which will cause a sharp rise in the overall aerodynamic resistance of the train; the total aerodynamic drag of the vehicle at −20 °C is about 14.9% higher than that under the 20 °C working condition.

2. With the drop of temperature, the downward pressure borne by the head car and the positive lift of the tail car will increase synchronously, and the change of these two vertical loads will break the original balance state of the vehicle longitudinal pitching moment.

3. Temperature change only adjusts the magnitude of pressure distribution on the vehicle surface, and will not change the basic topological structure of the surrounding flow field such as flow separation position and vortex distribution form. The expansion of the high-pressure stagnation area on the head car and the enhancement of the negative pressure area on the roof under low temperature are the direct flow field causes of the growth of each aerodynamic load.

Combined with the above research results, this paper suggests that the temperature correction coefficient should be added to the traction force calculation and vehicle safety evaluation process of high-speed trains operating in cold regions, so as to realize more accurate prediction of vehicle aerodynamic performance. Subsequent research work can further introduce icing, snow accumulation and other environmental factors to explore the coupling influence of multiple cold climate factors on the aerodynamic characteristics of trains.

References

[1] Han, Y., Chen, D., Liu, S., et al. (2020). An investigation into the effects of the Reynolds number on high-speed trains using a low temperature wind tunnel test facility. *Fluid Dynamics & Materials Processing, 16*(1), 1-19.

[2] Dai, Z., Li, T., Zhang, W., et al. (2024). Research on the aerodynamic characteristics of high-speed trains in different altitude environments. *Journal of Mechanical Engineering, 60*(16), 291-305.

[3] Du, J., Liang, X., Li, G., et al. (2020). Numerical simulation of rainwater accumulation and flow characteristics over windshield of high-speed trains. *Journal of Central South University, 27*, 198-209.

[4] Wang, F., Guo, Z., Shi, Z., et al. (2023). A study of crosswind characteristics on aerodynamic performance of high-speed trains on embankment. *Iranian Journal of Science and Technology, Transactions of Mechanical Engineering, 47*, 417-431.

[5] He, X., Zuo, T., Zou, Y., et al. (2020). Experimental study on aerodynamic characteristics of a high-speed train on viaducts in turbulent crosswinds. *Journal of Central South University, 27*, 2465-2478.

[6] Liu, T., Chen, Z., Zhou, X., et al. (2018). A CFD analysis of the aerodynamics of a high-speed train passing through a windbreak transition under crosswind. *Engineering Applications of Computational Fluid Mechanics, 12*(1), 137-151.

[7] Zhao, H., Zhai, W., Chen, Z. (2015). Effect of noise barrier on aerodynamic performance of high-speed train in crosswind. *Wind and Structures, 20*(4), 509-525.

[8] Suzuki, M., Tanemoto, K., Maeda, T. (2003). Aerodynamic characteristics of train/vehicles under cross winds. *Journal of Wind Engineering and Industrial Aerodynamics, 91*(1-2), 209-218.

[9] Suzuki, M., Hibino, Y. (2016). Field tests and wind tunnel tests on aerodynamic characteristics of train/vehicles under crosswinds. *Quarterly Report of RTRI, 57*(1), 55-60.

[10] Zhang, J., He, K., Xiong, X., et al. (2017). Numerical simulation with a DES approach for a high-speed train subjected to the crosswind. *Journal of Applied Fluid Mechanics, 10*(5), 1329-1342.